membranes

MDPI

Article

Investigating Structural Dynamics of KCNE3 in Different Membrane Environments Using Molecular Dynamics Simulations

Isaac K. Asare[1], Alberto Perez Galende[1], Andres Bastidas Garcia[1], Mateo Fernandez Cruz[1], Anna Clara Miranda Moura[1], Conner C. Campbell[1], Matthew Scheyer[1], John Paul Alao[2], Steve Alston[1]. Andrea N. Kravats[2], Charles R. Sanders[3], Gary A. Lorigan[2*], Indra D. Sahu[1,2*]

[1] Natural Science Division, Campbellsville University, Campbellsville, Kentucky.
[2] Department of Chemistry and Biochemistry, Miami University, Oxford, Ohio.
[3] Department of Biochemistry and Center for Structural Biology, Vanderbilt University, Nashville, Tennessee.
* Correspondence: idsahu@campbellsville.edu, Tel.: (270) 789-5597 (IDS); gary.lorigan@miamioh.edu, Tel.: (513) 529-2813 (GAL)

Abstract: KCNE3 is a potassium channel accessory transmembrane protein that regulates the function of various voltage-gated potassium channels such as KCNQ1. KCNE3 plays an important role in the recycling of potassium ion by binding with KCNQ1. KCNE3 can be found in the small intestine, colon, and in the human heart. Despite its biological significance, there is little information on the structural dynamics of KCNE3 in native-like membrane environments. Molecular dynamics (MD) simulations are a widely used as a tool to study the conformational dynamics and interactions of proteins with lipid membranes. In this study, we have utilized all-atom molecular dynamics simulations to characterize the molecular motions and the interactions of KCNE3 in a bilayer composed of: a mixture of POPC and POPG lipids (3:1), POPC alone, and DMPC alone. Our MD simulation results suggested that the transmembrane domain (TMD) of KCNE3 is less flexible and more stable when compared to the N- and C-termini of KCNE3 in all three membrane environments. The conformational flexibility of N- and C- termini varies across these three lipid environments. The MD simulation results further suggested that the TMD of KCNE3 spans the membrane width having residue A69 close to the center of the lipid bilayers and residues S57 and S82 close to the lipid bilayer membrane surfaces. These results are consistent with previous biophysical studies of KCNE3. The outcomes of these MD simulations will help design biophysical experiments and complement the experimental data obtained on KCNE3 to obtain a more detailed understanding of its structural dynamics in the native membrane environment.

Keywords: KCNE3, structural dynamics, lipid bilayers, molecular dynamics simulation, membrane mimetic

Citation: Asare, I.K.; Galende, A.P.; Garcia, A.B.; Cruz, M.F.; Moura, A.C.M.; Campbell, C.C.; Scheyer, M.; Alao, J.P.; Kravats, A.N.; Sanders, C.R.; et al. Studying Structural Dynamic Properties of KCNE3 in Different Membrane Mimetic Systems Using Molecular Dynamics Simulations. *Membranes* **2022**, *12*, x. https://doi.org/10.3390/xxxxx

Academic Editor(s):

Received: date
Accepted: date
Published: date

1. Introduction

KCNE3 is a potassium channel accessory transmembrane protein belonging to the KCNE family that regulates the function of various voltage-gated potassium channels such as KCNQ1 and KCNQ4 *(1-4)*. KCNE3 has been expressed in the small intestine, colon, and human heart *(5-7)*. Previous studies have shown that in the presence of KCNE3, KCNQ1's voltage sensitivity shows a linear current-voltage (I-V) relationship that gives rise to a potassium ion conductivity in non-excitable cells as polarized epithelial cells of the colon, small intestine, and airways *(3, 8, 9)*. Its malfunction has been proven to contribute to health disorders such as cardiac arrhythmia, long QT syndrome, tinnitus, cystic fibrosis, and Menière's disease *(3, 5, 10-15)*. For such a biologically significant membrane protein, little information is known about the structural and dynamic

properties of KCNE3 in native like membrane environment, where interactions between lipids and proteins help stabilize the structure of the protein and influence protein function within the membrane. Previous NMR studies of KCNE3 in detergent micelles and isotropic bicelles by the Sanders lab have shown KCNE3's structure consists of an extracellular N-terminus surface associated amphipathic helix connected by a loop to an alpha helical transmembrane domain *(16)*. A disordered C-terminus is connected to the transmembrane domain by a short juxta membrane helix *(16)*. Recent studies by Sun et al. using cryo-electron microscopy (Cryo-EM) showed that KCNE3 tucks its single membrane spanning helix against KCNQ1 at a point that appears to keep the voltage sensor in its depolarized confirmation *(8)*. However, it is not fully understood how these various sections behave structurally and dynamically in various membrane bilayer environments.

Molecular dynamics (MD) simulations serve as a structure biology tool to complement experimental studies in order to study the stability and structural dynamic properties of membrane proteins at an atomic level *(17-21)*. Here, we use all-atom MD simulations in the course of 105 ns to study stability and structural dynamic properties of KCNE3 in bilayers composed of POPC (1-palmitoyl-2-oleoyl-*sn*-glycero-3-phosphocholine)/POPG (1-palmitoyl-2-oleoyl-*sn*-glycero-3-phospho-(1'-*rac*-glycerol) (sodium salt)) (3:1), POPC alone, and DMPC (1,2-dimyristoyl-sn-glycero-3-phosphocholine) only. The POPC/POPG mixtures, POPC alone and DMPC are widely used lipid systems to mimic biological membrane bilayers for biophysical studies *(16, 17)*. Previous MD simulation studies on similar membrane proteins and other protein systems have suggested that the simulation times of 10-100 ns can provide reliable analysis of protein-detergent and protein-lipid interactions *(17, 22-24)*. We have analyzed MD simulation trajectory data to obtain several structural dynamics related parameters such as backbone root mean square deviation (RMSD), root mean square fluctuation (RMSF), lipid bilayer membrane width, Z-distances, total protein-lipid interaction energy, TMD helical tilt angle, and a heat map of the correlation between parameters, results that yield insight into the stability, molecular motion and interaction of KCNE3 in different phospholipid bilayer membranes.

2. Methods

2.1 Molecular Dynamics modeling of wild-type KCNE3 in Lipid Bilayers

Nanoscale molecular dynamics (NAMD) *(25)* version 2.14 with the CHARMM36 force field was employed to perform molecular dynamics simulations on a full length KCNE3 (PDB ID: 2M9Z, the original pdb file is available in the Supporting Information of the ref. *16)* in lipid bilayers composed of POPC/POPG (3:1), POPC alone, and DMPC alone *(26-28)*. The simulation set up and input files were generated by using CHARMM-GUI (http://www.charmm-gui.org) *(29)*. The visual molecular dynamics software (VMD) Xplor version 1.13 *(30, 31)* was used for MD trajectory data analysis. The bilayer, composed of a pre-equilibrated lipid molecules with a ~12,010.5 $Å^2$ surface, was built using membrane builder protocol under CHARMM-GUI *(29, 32)*. The total charge of KCNE3 was 2.0 in the simulation. The positively charged amino acid residues were protonated and negatively charged amino acids were deprotonated. The histidine (HIS) residues were protonated to the neutral form *(*HSD*)*. The protein was inserted into the membrane and the system was solvated into a TIP3 water box and ionized to add bulk water above and below the membrane and to neutralize the system with KCl using the membrane builder protocol *(29, 32)*. The final assembled system comprised waters, phospholipids, ions and the protein (a total of ~ 174,071 atoms). Six equilibration steps of equilibration of the system were performed for 50ps-200ps, 2fs timesteps with NAMD using the input files generated by CHARMM-GUI before running production run following the instructions provided in the membrane builder protocol *(29, 32)*. The minimization equilibration inputs utilized collective variable restraints to slowly release the

system to facilitate stable simulation. Starting from this equilibrated system, NAMD simulations were carried out to ~ 105 ns using Langevin dynamics for the three membrane environments *(18)*. Electrostatic interactions were computed using the Particle-Mesh Ewald algorithm with a 12 Å cutoff distance *(33)* and Van der Waals interactions were computed with a 12 Å cutoff distance and a switching function to reduce the potential energy function smoothly to zero between 10-12 Å. Periodic-boundary conditions were used and constant temperature (303 K) and pressure (1 atm) were maintained. Equations of motion were integrated with a timestep of 2 fs and trajectory data were recorded in 20 ps increments *(18)*.

2.2 Analysis of the MD simulation data

The structures in the MD trajectory data were aligned with respect to the first structure for each membrane bilayer environment before further analysis. The stability and structural dynamic behavior of KCNE3 was obtained from the aligned trajectory data by calculating root mean square deviation (RMSD) of all atoms of the backbone, root mean square fluctuation (RMSF), lipid bilayer membrane width, Z-distances, total protein-lipid interaction energy, and TMD helical tilt angle using the scripts available in the VMD software package *(30)*. The heatmaps for the correlation between different simulation parameters were graphed using Matlab (https://www.mathworks.com). The images were prepared using the Igor Pro graphics program (https://www.wavemetrics.com). All molecular dynamics simulations were run on the Miami Redhawk cluster computing facility at Miami University.

3. Results and Discussions

The stability and structural dynamic properties of KCNE3 in different phospholipid bilayer environments were investigated using NAMD molecular dynamics simulation trajectory data. A wild-type KCNE3 protein was incorporated into three different lipid bilayer environments including POPC/POPG (3:1), POPC alone, and DMPC alone to study how structural and dynamic properties of KCNE3 behave in different lipid bilayer environments. In this study, we utilized individual lipids and a mixture, where POPC and POPG are monounsaturated lipids and DMPC is saturated lipid. These lipids are widely used in studying membrane protein/peptides. POPG lipids contain a negative charge and hence the mixture of POPC and POPG at the molar ratio of 3 to 1 may provide more favorable condition to stabilize the TMD of KCNE3 buried into lipid bilayers while spanning the width of the bilayer membrane *(34, 35)*. Figure 1 shows the chemical structure of lipids, the NMR structure of KCNE3 incorporated into POPC/POPG and solvated into water and the amino acid sequence of the wild-type KCNE3 with distribution of charged amino acids by color codes *(16)*.

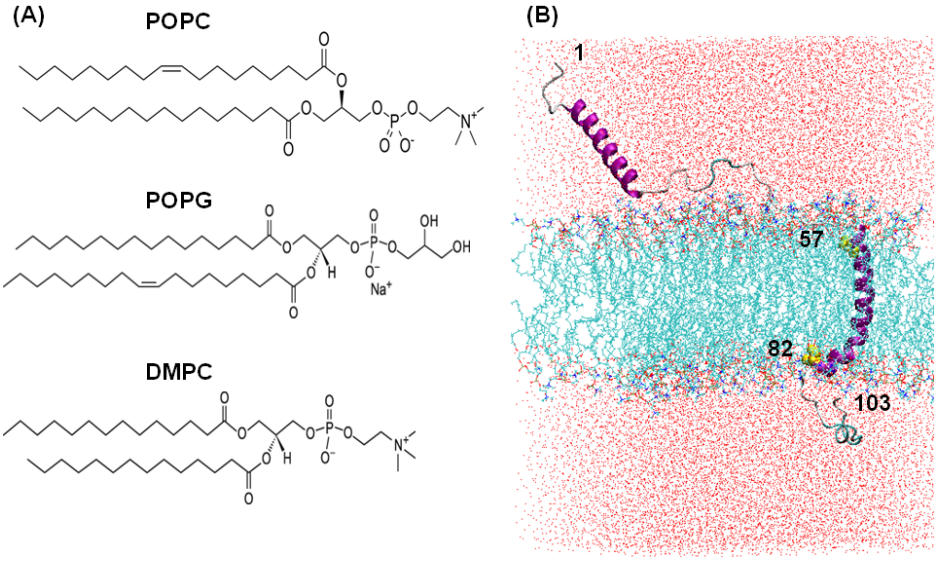

(C)

Wild-type KCNE3 amino acid sequence:

^{1}METTNGTET^{10}WYESLHAVLKALNATLHSNLL^{31}CRPGPGLGPDNQ

^{43}TEERRASLPGRDDN^{57}SYMYI LFVMFLFAVTVGSLILGYTRS^{83}RKV

DKRS^{90}DPYHVY^{97}KNRVSMI

Figure 1. (A) Chemical structure of phospholipids used for the NAMD molecular dynamics simulations. **(B)** An illustrative example of the cartoon representation of the NMR structure of KCNE3 (PDB ID: 2M9Z) incorporated into POPC/POPG lipid bilayers and solvated into water box *(16)*. Amino acid sites 1-56 represent N-terminus, amino acid sites 57-82 represent TMD and sites 83-103 represent C-terminus. The amino acid sites 57 and 82 are colored yellow.(C) Amino acid sequence of the wild-type KCNE3 with distribution of charges. Positive charges (Red), negative charges (Blue), and Histidine (Green) are color coded. The highlighted red box represents the transmembrane domain and blue boxes represent N- and C-terminal helices.

Molecular motion of KCNE3 in different phospholipid bilayer environments

An all-atom molecular dynamics simulation on wild-type KCNE3 in three different lipid bilayer environments was carried out over the course of 105 ns. Figure 2 shows the snapshots of the representative MD simulation output trajectory data of KCNE3 incorporated into all three lipid bilayer systems (POPC/POPG, POPC alone, and DMPC alone) for 16 ns, 40 ns, 80 ns and 105 ns. The interaction of C- and N-termini of KCNE3 with lipid bilayer surface is flexible and dynamic for all three lipid compositions. Interestingly, the initial few amino acid sites of N-terminal of KCNE3 showed a short beta sheet structure for the DMPC lipid system.

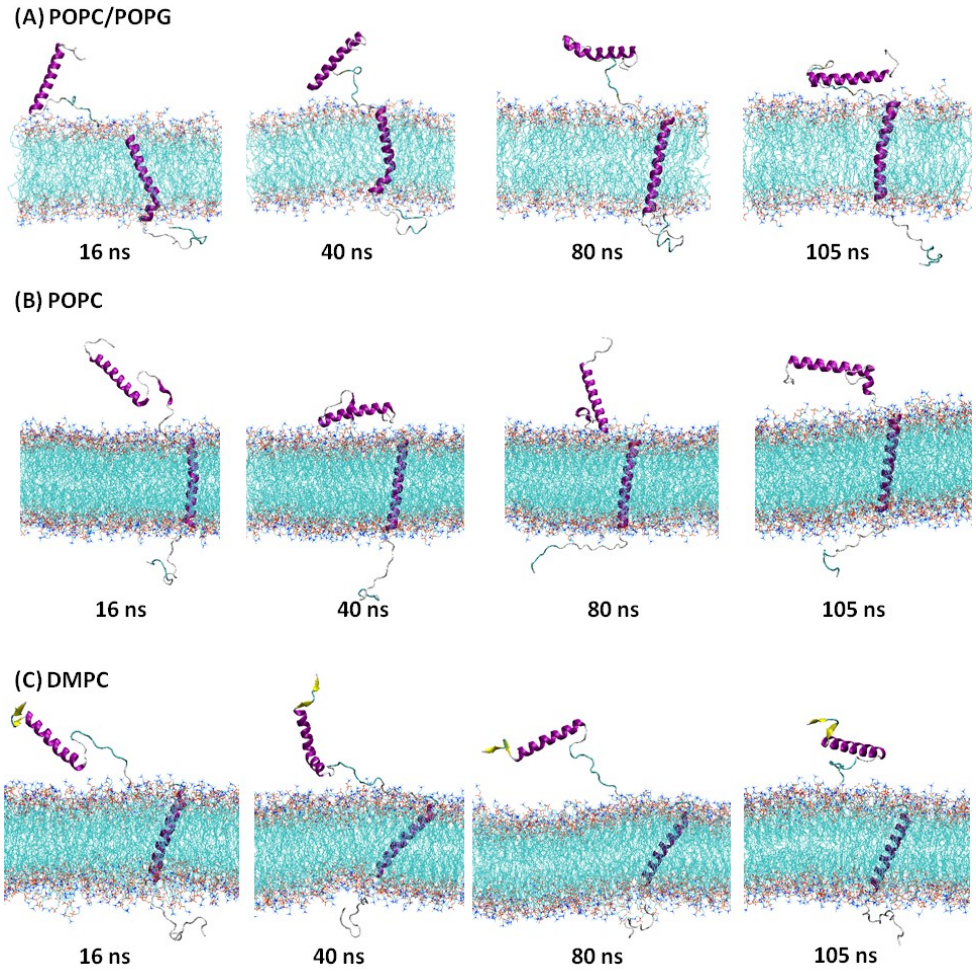

Figure 2. Snapshots of the representative MD simulation trajectory data of KCNE3 at 16 ns, 40 ns, 80 ns, and 105 ns for POPC/POPG **(A)**, POPC alone **(B),** and DMPC alone **(C)** lipid bilayers. The hydrogen atom and water are omitted to make visualization simple and clear.

In order to analyze the conformational stability and molecular motion of the wild-type KCNE3 in membrane environments, a backbone root mean square deviation (RMSD) was calculated from the trajectory data and plotted as a function of simulation time for different segments of the protein including transmembrane domain (TMD), C-terminus, N-terminus, C-terminal helix, and N-terminal helix for POPC/POPG (3:1), POPC alone, and DMPC lipid bilayers as shown in Figure 3. We omitted analysis of the first 15 ns of each trajectory of the production run to avoid the equilibration time of the system. The RMSD measures the mean position of the amino acid residues in the structure of the subsequent simulation frames and compares them to the initial structure *(22)*. The RMSD is important in identifying regions of the proteins that has higher flexibility as well as regions that are stabilized. The initial trajectories for all simulations in the POPC/POPG and POPC alone systems are similar. The RMSD profile pattern for POPC/POPG (Figure 3A) shows that the RMSD values for the TMD of KCNE3 are lower than that of N-terminus and N-terminal helix until 49 ns and then increases to have similar values by 105 ns. The RMSD values for C-terminal and C-terminal helix are lower than the that of the TMD, N-terminus and N-terminal helix and varying within the whole simulation range. Similarly, the RMSD profile pattern for POPC (Figure 3B) shows that the RMSD values for the TMD of KCNE3 are very close to that of N-terminus and N-terminal helix during the whole simulation range. The RMSD values for the C-terminal helix are relatively lower than the TMD, N-terminus and N-terminal helix and C-terminus with fluctuating values. The RMSD values for the C-terminus are also close to these values but highly fluctuating within the whole simulation range. Similarly, the RMSD profile pattern for DMPC (Figure 3C) shows that the RMSD values for the TMD, N-terminus, N-terminal helix, C-terminal helix, and C-terminus are closely varying to each other with the RMSD values for the C-terminus is also highly flexible within the whole simulation range. KCNE3 appears to be

more stable in DMPC than in POPC/POPG or POPC alone, as the RMSD profiles for each segment are suppressed by comparison. In the POPC/POPG and POPC alone systems, it is observed that the N-terminus and N-terminal helix have the highest RMSDs of all the segments of KCNE3. These data suggest that these regions of the protein have conformationally higher backbone fluctuations in the KCNE3 structure. This is expected as the N-terminus contains a larger number of amino acid residues compared to the C-terminus and the TMD *(16)*. In the POPC/POPG and POPC alone systems, the RMSD values of the TMD starts out higher than that of the C-terminus and C-terminal helix. However, it is seen that the C-terminus and C-terminal helix have more varied fluctuations as compared to the TMD, suggesting that the C-terminus is more mobile and unstable as compared to the TMD. The overall fluctuations of the C-terminus are however lower than that of the N-terminus. The relatively smaller fluctuations observed for the TMD throughout the simulation suggests that it is the most stable segment of the protein and with the greatest stability of all segments studied. In the DMPC membrane mimetic system, the TMD is observed to have similar backbone fluctuations as in the POPC/POPG and POPC alone systems. However, the C-terminus segment starts out with the higher RMSD than that of the N-terminus in contrast to the other two POPC/POPG and POPC alone systems. Similarly, higher backbone fluctuations for N- and C-termini reveal a similar level of conformational instability in the DMPC bilayer system. The average RMSD values for different segments of the KCNE3 are also calculated for all three lipid systems from the data in Figure 3 and shown in Table1. The average RMSD values varies between 10.4 Å-23.5 Å for POPC/POPG, 10.3 Å to 17.4 Å for POPC alone, and 9.5 Å-15 Å for DMPC. The average RMSD value for the TMD in DMPC is the least value for TMD of the all three lipid systems studied. The C-terminal helix has the lowest average RMSD value when compared to different segments of the protein in all three corresponding lipid systems. The standard deviation calculated on the average RMSD data show higher values for the outside regions of the protein compared to the TMD in all three corresponding lipid system. The RMSD data for different regions of KCNE3 in different lipid bilayer environments suggest that the backbone flexibility for different segments of KCNE3 is different in POPC/POPG, POPC alone, and DMPC bilayer membranes. Our overall RMSD data suggest that the regions of the KCNE3 that is outside the membrane or interact with the surface are more flexible and DMPC lipid system plays more stabilizing role.

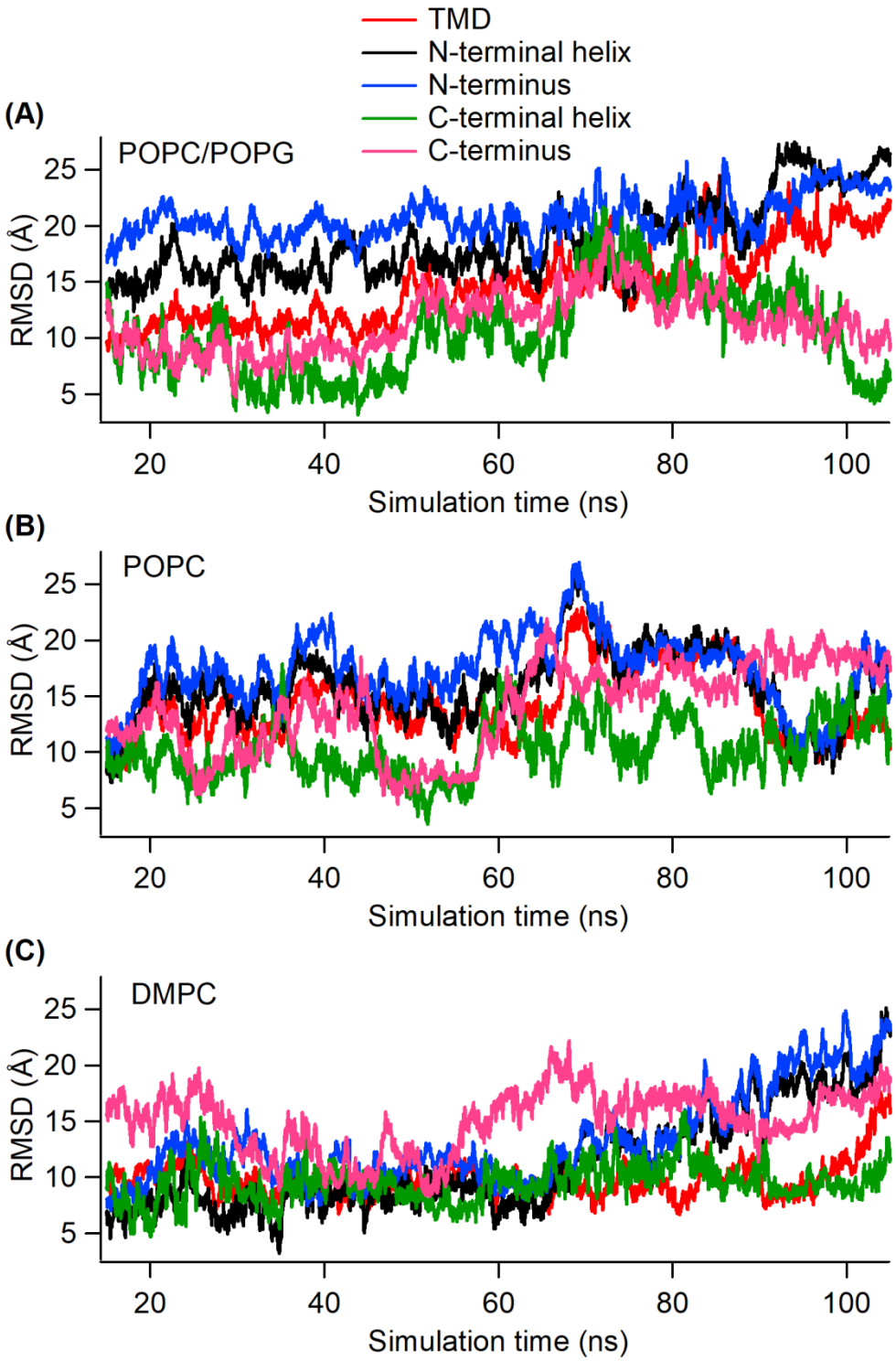

Figure 3. Root mean square deviation (RMSD) as a function of simulation time for different segments of KCNE3 in POPC/POPG **(A)**, POPC alone **(B)**, and DMPC **(C)**.

Table 1. Average RMSD calculated from the RMSDs shown in Figure 3. The error represents standard deviation.

	Average RMSD (Å)		
	POPC/POPG	**POPC**	**DMPC**
TMD	14.7 ±3.5	14.2±3.1	9.7±1.6
N-terminal helix	18.6±3.5	15.9±3.3	11.3±4.4

N-terminus	23.5±3.8	17.4±3.1	13.3±4.0
C-terminal helix	10.4±4.0	10.3±2.5	9.5±1.6
C-terminus	11.3±2.6	14.0±3.9	15±2.8

The RMSD data only provide the average behavior of the motion of the different segments of the protein while interacting with lipid bilayer membrane. We also wanted to understand how the flexibility of the particular regions assessed above contributed to the overall fluctuations that disturb the KCNE3's stability. The residue-wise fluctuation of different segments of bilayer-integrated KCNE3 while incorporated into lipid bilayers were quantitatively determined by the root mean square fluctuation (RMSF) as a function of simulation time as shown in Figure 4. While the RMSD indicates positional differences of entire structures over the course of the simulation, the RMSF calculates how much a residue fluctuates during the simulation *(22)*. Consequently, it helps determine the flexibility of individual residues. Figure 4 shows the RMSF for KCNE3 residues in the three bilayer conditions. The profile for KCNE3 is similar for all three bilayer compositions. Overall, residues 1-9 (unstructured region) and ~25-35 (around the terminal of N-terminal helix) of the N-terminus and residues ~96-103 (unstructured region) of the C-terminus have the largest RMSF, suggesting they are the most flexible.

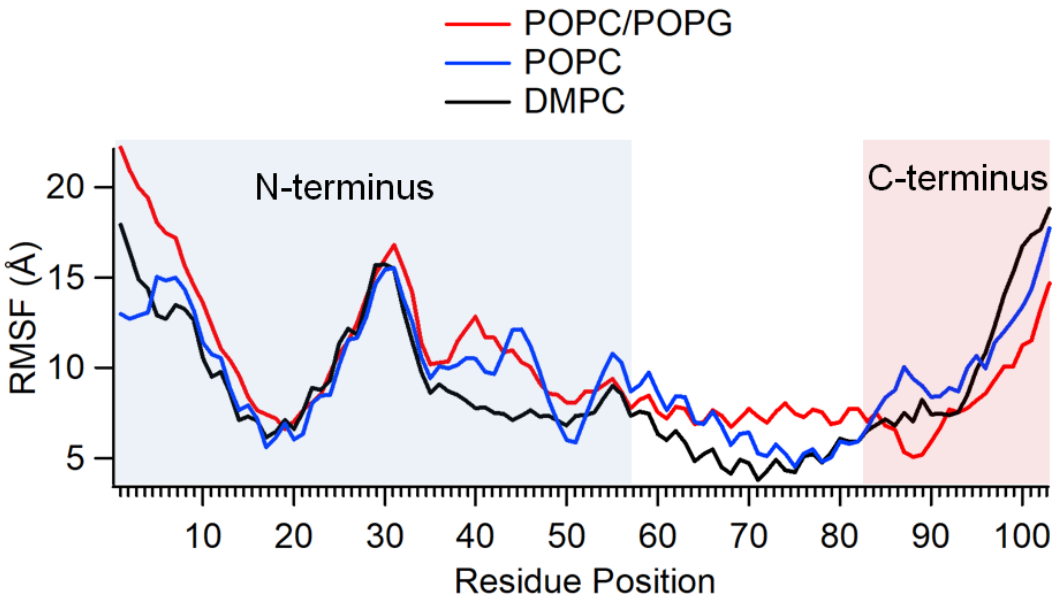

Figure 4. Plot of the root mean square fluctuation (RMSF) of KCNE3 as a function of simulation time for three different lipid compositions: POPC/POPG (Red), POPC (Blue), and DMPC (Black).

These results agree with the RMSD calculations that highlighted the highest fluctuations in the C- and N- termini. The RMSF of N-terminal residues 11-24 (helical region) and the TMD section from residue 57-82 are lower and indicate stability. The smallest RMSF fluctuations of the TMD region occur in DMPC, which is in agreement with our observations regarding the RMSD of this region. The previous NMR data-restrained molecular dynamics simulation on KCNE3 in DMPC lipid bilayers suggested the dynamic interaction of N- and C-termini helices with membrane surface *(16)*. These helices contain amphipathic amino acid sequence that do not deeply bury into the lipid bilayers and hence these helices can dynamically interact with surfaces. The fluctuation of different segments of KCNE3 as suggested by the RMSF plot is consistent with the RMSD data and

earlier NMR studies *(16)*. Our RMSF data suggest the N- and C-termini are more flexible with higher RMSD values in all three lipid compositions.

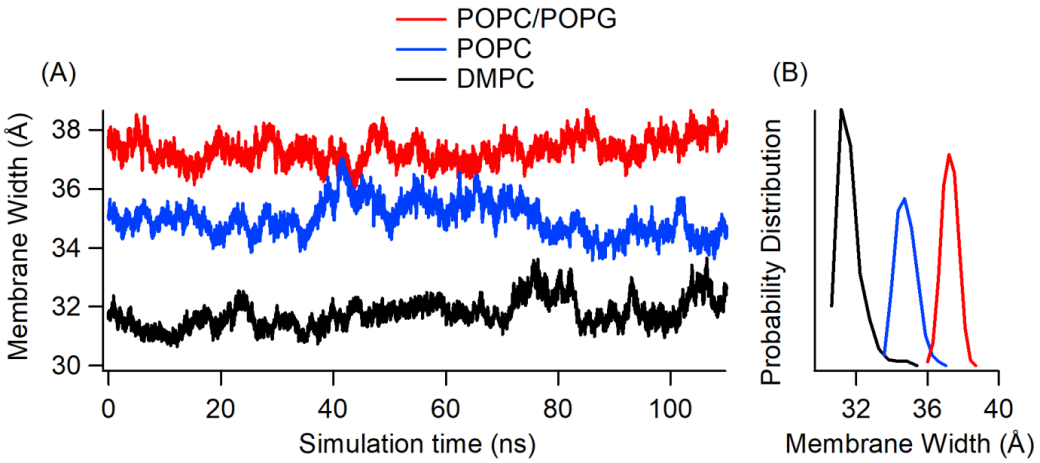

Figure 5. Membrane bilayer width incorporating KCNE3 protein as a function of simulation time **(A)** and membrane width probability distribution for POPC/POPG (Red), POPC (Blue), and DMPC (Black) bilayers.

We wanted to better understand the formation of the lipid bilayer in the presence of reconstituted KCNE3, since we observed a suppressed RMSD for the KCNE3 TMD region with DMPC, in comparison to POPC/POPG and POPC alone. Both tails of DMPC only have 14 carbons, while POPC and POPG have 16 and 18. We measured the width of the membrane bilayer as a function of the simulation time for all three membrane mimic environments (POPC/POPG, POPC alone, and DMPC) to determine whether DMPC was forming compacted bilayers that stabilized the KCNE3 TMD. The membrane width was calculated by measuring the distance between the center of mass of the phosphorus of the upper and lower lipid head groups. The membrane width is shown as a time series in Figure 5a, while the probability distribution of the timeseries data is represented in Figure 5b. The membrane width of DMPC is the lowest, as expected based on the length of hydrocarbon chains. The membrane width distribution plot (Figure 5B) shows the membrane width peak is centered around 37Å for POPC/POPG, 35Å for POPC and 31Å for DMPC. The membrane width for POPC/POPG lipid bilayers is thicker than that of POPC lipid bilayers, despite having the same number of carbon atoms in the acyl chains. Next, we wanted to understand the protein topology with respect to the lipid bilayer membrane, since we observed that each bilayer had a different membrane width. The membrane thickness is oriented about the Z-axis with the center of mass of the membrane bilayer located at Z=0. We calculated the distance from the Z-axis (Z-distance) of different segments of KCNE3 from the center of the mass of the lipid bilayers in all three different lipid membrane environments (POPC/POPG, POPC alone and DMPC). Previous NMR studies in micelles and isotropic bicelles suggested that amino acid residue sites 57 to 82 belong to the TMD of the KCNE3 that spans the membrane bilayer width *(16)*. The Z-distances of the center of mass of the N-terminal helix, residues S57, A69 and S82, and the C-terminal helix from the center of mass of the lipid bilayers were calculated from the MD trajectory data. These Z-distance data can provide us with the information on how much various residues and different segments in the protein structure moved away from the center of the lipid bilayers when incorporated into different membrane environments. Figure 6 shows the plot of Z-distance as a function of

simulation time for center of mass of different segments (N- and C-termini helices), and sites S57, A69, and S82 of TMD of KCNE3 in three different lipid bilayer environments (POPC/POPG, POPC alone, and DMPC). Figure 6A indicates that the TMD termini sites S57 and S82 are close to the surface of the lipid bilayer and span the width of the membrane for POPC/POPG lipid bilayers. Figure 6A shows that the amino acid residue site A69 lies close to the center of the lipid bilayers for POPC/POPG as indicated by the Z-distance around zero. The Z-distance for N- and C-termini helices vary outside the membrane width range. Similar trend of Z-distance pattern profile was observed for POPC alone and DMPC lipid bilayer environments. However, the Z-distance ranges for the TMD termini residues S57 and S82 for DMPC is lower than that for POPC/POPG and POPC alone. This is expected as the DMPC bilayer width is lower than that of the POPC/POPG and POPC alone(Figure 5). The behavior of Z-distance pattern profile for these lipid bilayer environments are consistent with the membrane width profile shown in Figure 5.

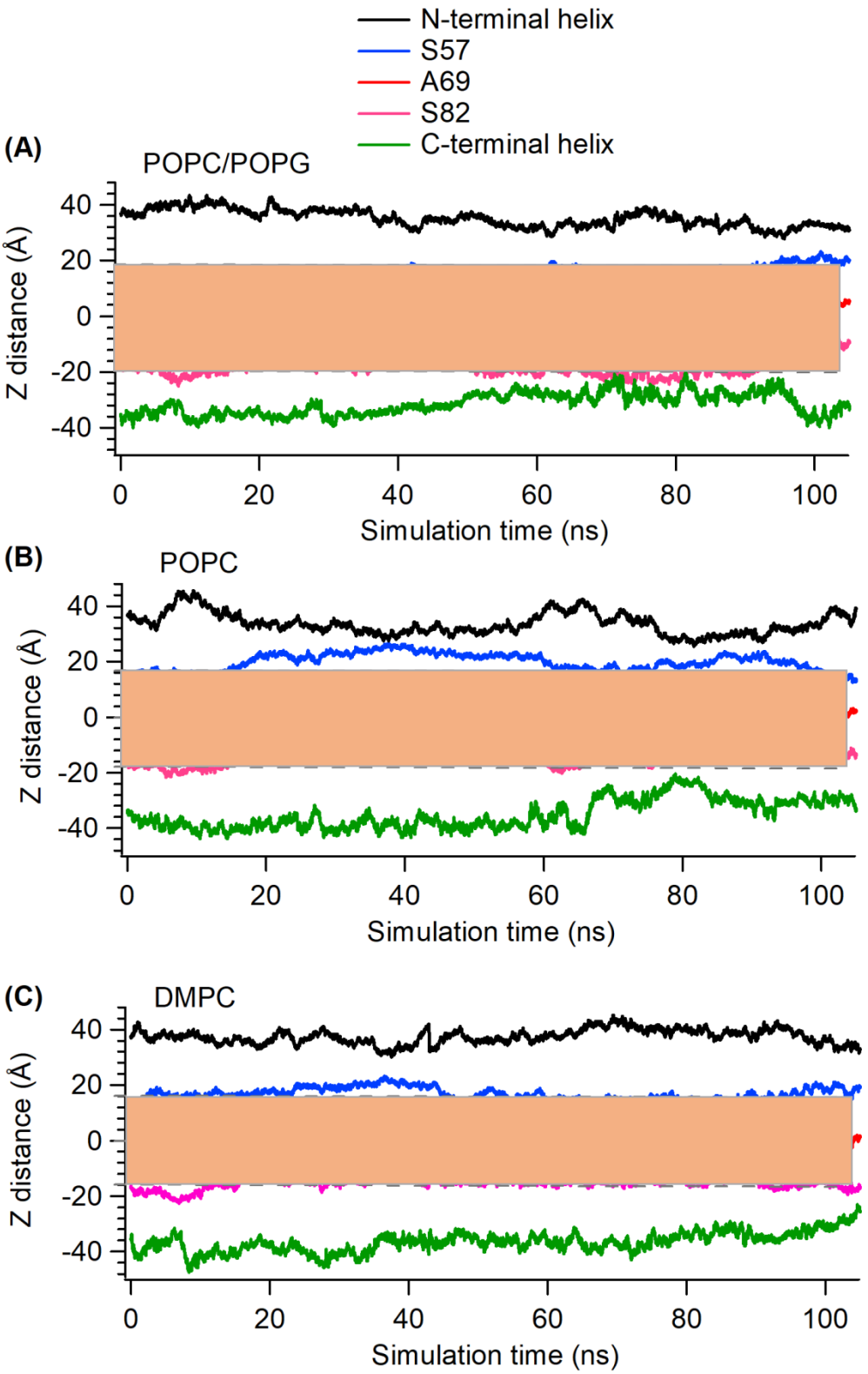

Figure 6. The plot of Z-axis distance (Z-distance) as a function of simulation times for KCNE3 incorporated into POPC/POPG **(A)**, POPC **(B)**, and DMPC **(C)** lipid bilayers. Shaded regions represent the average width of the corresponding lipid bilayers calculated from Figure 5.

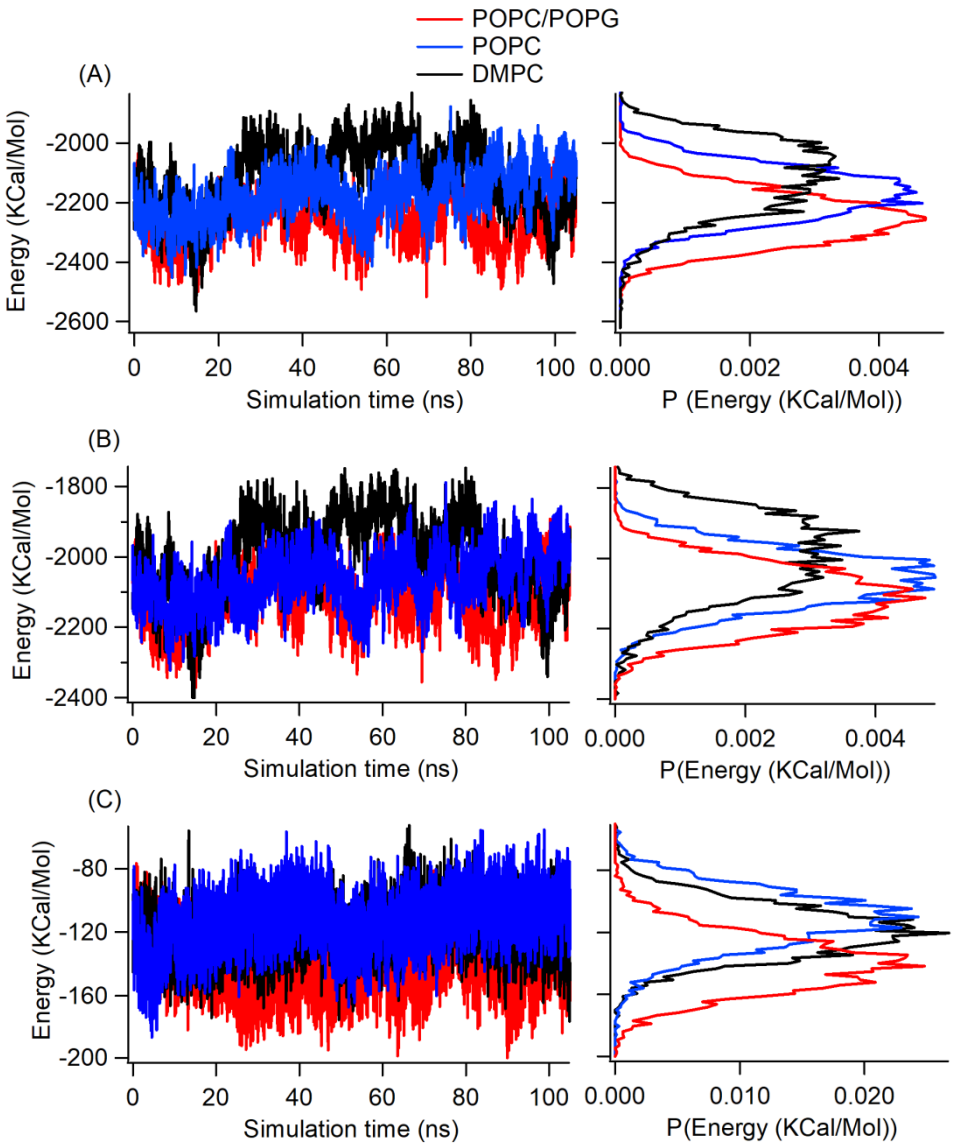

Figure 7. Internal **e**nergy of KCNE3 in lipid bilayer membranes as a function of simulation time (left panel) and corresponding histogram (right panel) for total internal energy **(A),** electrostatic energy **(B)** and van der Waals energy **(C).** The x-axis of the histogram plot represents probability distribution. The bin of 85 was used to obtain histogram.

In order to understand the stability of the interaction of the KCNE3 reconstituted into lipid bilayer membrane environments, we calculated the internal energy of KCNE3 and plotted this energy as a function of simulation time for all three membrane bilayer environments and corresponding histograms for total internal energy, electrostatic energy contribution and van der Waals energy contribution as shown in Figure 7. Figure 7A shows similar total energy profiles for all three systems. When the data is represented as a probability distribution (right panel), the total internal energy of the KCNE3 is the lowest, with more favorable values in the POPC/POPG lipid bilayers. The total internal energy of KCNE3 increases for POPC bilayers and is the least favorable in DMPC. Figure 7B shows the similar internal energy trends and histogram profiles for electrostatic energy contribution when compared to the total energy profile for all three systems. Figure 7C shows a lower van der Waals contribution to the total internal energy when compared to the electrostatic energy contribution. The probability distribution (Figure 7C, right

panel) shows the van der Waals energy of KCNE3 has a slightly lower value in POPC/POPG lipid bilayers when compared to the POPC alone and DMPC alone systems both having similar van der Waals energy contributions. The electrostatic interactions are the dominant contribution to the total energy for all three lipid environments. The trend of the total internal energy in all three lipid environments suggests that the overall protein structure is more stable in POPC/POPG bilayer membrane compared to the cases of POPC and DMPC. Our hypothesis is that when the KCNE3 is unable to interact with the lipids, it relies on internal interactions to stabilize the structure.

To test this hypothesis, we computed the interaction energy of different segments of the KCNE3 with the lipid bilayer membrane as shown in Figure 8. In all three lipid environments, the interaction energy of the TMD section with the lipid is lower than that of C-terminus, C-terminal helix, and N-terminal helix with the lipid. The interaction energy of the N-terminus is close to interaction energy of the TMD but fluctuates throughout the whole simulation time. While the interactions of the N- and C- termini appear to be strong and exhibit large fluctuations, the N- and C-termini helices weakly interact with the lipid. Inspection of the trajectory data suggests these helices are closely interacting with the membrane surface during the simulation time where interaction energy attains lowest values. The average interaction energies for each section of KCNE3 during the whole simulation trajectories were calculated for all three lipid systems from the interaction energy data (Figure 8) as shown in Table 2. The average interaction energy for the TMD of KCNE3 has a similar value (within the error) for all three lipid systems. Similarly, other segments of the protein have similar average interaction energy (within the error) in all three corresponding lipid systems. However, the standard deviation values are larger for the N- and C-termini in all three lipid systems. These data suggest that the interactions of the N-and C-termini of KCNE3 with the membrane surface are dynamic.

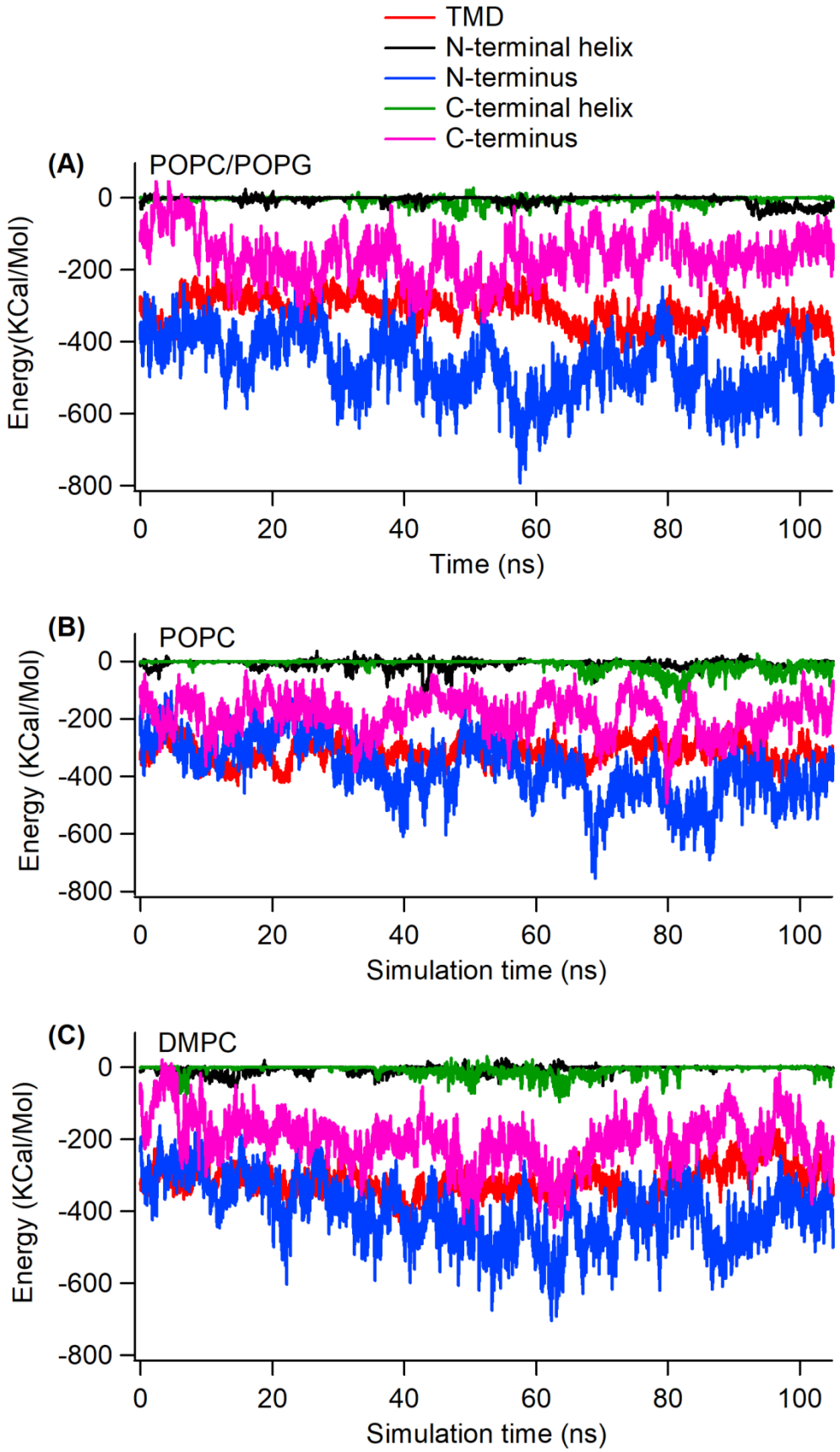

Figure 8. Interaction energy of different segments of KCNE3 with lipid bilayer membranes as a function of simulation time for POPC/POPG **(A)**, POPC **(B)**, and DMPC **(C)** lipid bilayers.

These interaction energy data suggest that the N-terminus interacts most strongly with the membrane surface but the interaction is dynamic and unstable, as the standard deviation in the average energy calculation is very high for this segment of the protein. While the interaction energy of TMD is higher than that of the N-terminus, the stability of the TMD structure might be coming from the internal energy of the protein and also its transient contact with water *(16)*.

Table 2. Average interaction energy calculated from the interaction energy shown in Figure 8. The error represents standard deviation.

	Average Interaction Energy (KCal/Mol)		
	POPC/POPG	**POPC**	**DMPC**
TMD	-313.7 ±42.3	-316.6±37.5	-317.5±42.2
N-terminal helix	-5.6±10.9	-8.0±14.8	-5.4±9.4
N-terminus	-465.3±85.3	-371.8±105.3	-401.3±86.8
C-terminal helix	-4.9±8.8	-11.6±20.2	-7.5±13.7
C-terminus	-162.5±64.5	-184.7±63.7	-200.6±68.5

To better understand the conformational stability and the interaction of the transmembrane domain (TMD) of KCNE3 with membrane bilayers, we calculated the helical tilt of the TMD within the bilayer. In our previous results, we saw that the membrane thickness was dependent upon the lipid environment, though there were minute differences in the z-distances of the terminal residues of the TMD helix. We wanted to establish whether the deformation of the helix occurred in order to accommodate the structure within the bilayer. We have plotted the probability density of the transmembrane (TM) helical tilt of KCNE3 with the membrane normal and the Z-distance of the TMD of KCNE3 from the center of the mass of lipid bilayers for all three different membrane environments (POPC/POPG, POPC alone, and DMPC) as shown in Figure 9. The initial Z-distance mostly fluctuated around 0 Å. When KCNE3 is embedded in the POPC/POPG lipid bilayer, two conformations of the TMD helix are observed; the dominant population is centered around a Z-distance of - 3Å and a helical tilt of 45° while the second less populated conformation is at a Z-distance of 2Å and a helical tilt of 75°. In the case of POPC alone, similar conformations are observed, though the populations are more diffuse with sampling of many intermediate states between the two dominant conformations in Figure 9 in a combination of POPC/POPG. By comparison, only one dominant conformation exists in the DMPC lipid, which is unique to DMPC and not observed in the other two lipid environments. The highest probability is centered around a Z-distance of 3.5Å, while the helical tilt fluctuates between 45° and 70°. These data suggest that there is a strong correlation between TM helical tilt angle and Z-distance for POPC/POPG bilayers and DMPC bilayers, and a weak correlation was observed for POPC bilayers. Interestingly, the dominant probability density for the DMPC membrane appears for the Z-distance of the TMD of around 4Å from the center of the mass of the bilayers and TM helical angle of around 45°-70°. This suggests that the TMD helix tilts in order to remain embedded within the lipid bilayers. However, in DMPC the TMD helix is more stationary at the Z-distance and samples less tilt angles, suggesting that it is more stable in this lipid system. In contrast, when the TMD helix is in POPC/POPG and POPC alone the tilting behavior of the TMD helix results in changes in Z-position, suggesting higher the TMD helix is more mobile within these lipids. These probability distribution patterns are also consistent with the membrane width data shown in Figure 5.

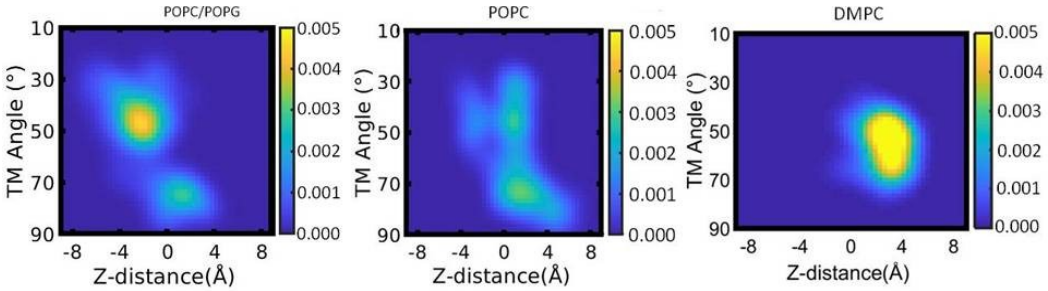

Figure 9. Probability density plot of transmembrane (TM) helical tilt angle against the Z-distance of TMD of KCNE3 in different lipid bilayer membranes. The yellow color indicates the highest probability and blue color represents the lowest probability.

We wanted to further understand the conformational stability and interaction of different segments of KCNE3 with membrane bilayers. We plotted the correlation between the total interaction energy of different segments of KCNE3 (N-terminus, N-terminal helix, TMD, C-terminal helix and C-terminus) and the corresponding Z-distances from the center of the mass of the membrane bilayers in Figure 10. Figure 10A shows the probability distribution for the N-terminus. Similar trends are observed for POPC/POPG and DMPC, with one dominant population that varies between Z-distances of 35-50 Å and interacts strongly with the lipids with energies ranging from -550 to -750 kcal/mol. Interestingly, the probability distribution for POPC alone is more dispersed and involves much lower interaction energies. Inspection of the visualization of the trajectory data suggests that the interaction of the N-terminus with the POPC membrane surface is dynamic and very unstable, with a wide spreading of its portion above the surface with occasionally anchoring to it. For the N-terminal helix of KCNE3 (Figure 10B), the probability distributions are similar for all three lipid environments. However, an additional disperse density with higher interactions and Z-distances closer to the head groups is observed for POPC/POPG. The inspection of the visualization of the trajectory data suggest that N-terminal helix also interact dynamically with the POPC/POPG membrane surface and develops a bending in the helix during the interaction during certain periods of simulation times. Similar trend of a dominant population for the TMD helix is observed for all three systems (Figure 10C). However, an additional dispersed density with higher interactions with same Z-distance has been observed in POPC. The probability density for the TMD helix also shows higher interactions in DMPC. For the C-terminal helix (Figure 10D) and the C-terminus (Figure 10E), similar populations are observed in all three lipid systems with a slightly weaker interactions observed in the POPC/POPG system. Together, these data suggest that the TMD of KCNE3 is stably interacting with all three lipid systems with DMPC conferring the greatest stability. While the N-terminus of POPC/POPG is interacting strongly, it is more dynamic and less stable. The interaction trend of C-terminus is similar in POPC alone and DMPC. The week interaction of C-terminus in POPC/POPG suggesting that the unanchored regions of the either termini are stabilized by the interactions with water. The probability density pattern for different segments observed in these three environments are consistent with our RMSD, RMSF, membrane width, Z-distances, and total interaction energy data (Figure 3-7).

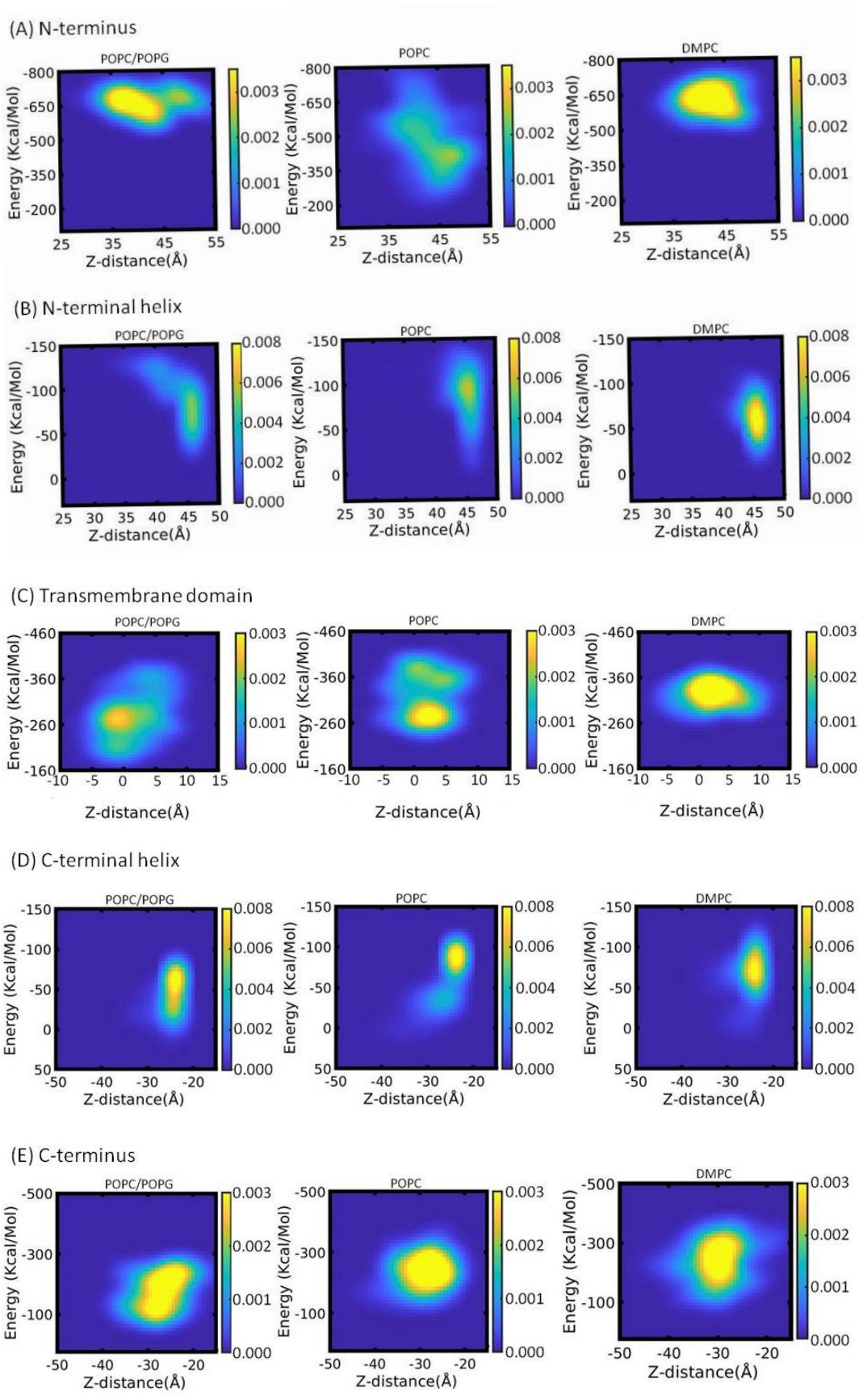

Figure 10. Probability density plot of total interaction energy of different segments of KCNE3 with lipid bilayers against corresponding Z-distances from the center of mass of the lipid bilayers for

different lipid bilayer membranes. The yellow color indicates the highest probability and blue color represents the lowest probability.

NMR studies by the Sanders lab on KCNE3 in LMPC (lyso-myristoylphosphatidyl choline) micelles and DMPG (dimyristoylphosphatidylglycerol)/ DHPC(dihexanoylphosphatidylcholine) isotropic bicelles have suggested that KCNE3 adopts a single α-helical transmembrane domain (57-81). This is connected to a flexible loop with N-terminal surface associated amphipathic helix (10-30) and a short juxtamembrane helix (90 to 95) and a disordered C-terminus (96 to 103) *(16)*. The previous double electron electron resonance (DEER) electron paramagnetic resonance (EPR) data on KCNE3 in POPC/POPG bilayered vesicles suggested that the TMD helix of KCNE3 adopts a moderate curvature with residues T71, S74, and G78 facing the concave side of the curvature *(16)*. The TMD of KCNE3 is crucial to its function and the curvature is important for binding to the activated-state channel *(16)*. A recent cryo-electron microscopic (Cryo-EM) spectroscopic study on the KCNE3-KCNQ1 complex in detergent micelles suggested that there is a deviation on the structure of KCNE3 interacting with KCNQ1 relative to the KCNE3 NMR structure model in isotropic bicelles with a root mean square deviation (RMSD) of 7.6 Å between the two structures *(8)*. Our all-atom molecular dynamics simulation data for 105 ns obtained on KCNE3 in POPC/POPG, POPC alone and DMPC bilayers reported in this study suggested that the center of mass of the KCNE3 TMD is slightly moved up and remained more stable in DMPC when compared to POPC/POPG and POPC alone while N- and C-termini are more conformationally flexible and interacting differently in all three environments. The N- and C-termini helices are also dynamically interacting with the solvent or may be partially interacting with the membrane surface. The MD simulation results further suggested that the TMD of KCNE3 spans the membrane bilayer width with the amino acid residue A69 situated close to the center of lipid bilayers and the residues S52 and S82 are close to the surface of the membrane bilayer. The total internal energy of KCNE3 suggested that the POPC/POPG lipid bilayer membrane provide more stable simulation and protein-membrane interaction. Our molecular dynamics simulation data are consistent with earlier experimental biophysical studies on KCNE3 *(8, 16, 36)*. Extending the MD simulation time longer than 105 ns may provide additional insight on the structural dynamic properties of KCNE3 while interacting with different mimetic systems.

4. Conclusions

All atom molecular dynamics simulations for 105 ns was performed on KCNE3 reconstituted into POPC/POPG, POPC alone and DMPC alone bilayer membrane environments to study the structural dynamic properties of KCNE3. The MD simulation results suggested that the TMD of the KCNE3 is less conformationally flexible and more stable when compared to the N- and C-termini in all three membrane environments. The N- and C-termini of KCNE3 are conformationally more flexible and dynamic in all these three lipid environments. The MD simulation results further suggested that the TMD of KCNE3 spans the membrane width having residue A69 being close to the center of the lipid bilayers and residues S57 and S82 being close to the apposing lipid bilayer membrane surfaces. These MD simulation results complement the experimental biophysical studies of KCNE3 in lipid bilayer membranes to illuminate its structural dynamic properties in more detail.

Funding: This work is generously supported by National Science Foundation NSF MCB-2040917 award. Gary A. Lorigan would like to acknowledge support from NSF (MRI-1725502) grant, NIGMS/NIH Maximizing Investigator's Research Award (MIRA) R35 GM126935 award, the Ohio Board of Regents, and Miami University. Gary A. Lorigan would also like to acknowledge support from the John W. Steube Professorship. Charles R. Sanders would like to acknowledge support from US NIH grant R01 HL122010.

Institutional Review Board Statement: Not applicable

Data Availability Statement: Not applicable

Acknowledgments: We would like to appreciate Dr. Jens Mueller, the Facility Manager Redhawk Cluster Miami University, for assistance with the computational work.

Conflicts of Interest: The authors declare no conflict of interest.

Abbreviations

MD, molecular dynamics;
RMSD, root mean square deviation;
RMSF, root mean square fluctuation;
LMPC, lyso-myristoylphosphatidyl choline;
DMPC, 1,2-dimyristoyl-sn-glycero-3-phosphocholine;
DHPC, dihexanoylphosphatidylcholine;
DMPG, dimyristoylphosphatidylglycerol;
POPC, 1-palmitoyl-2-oleoyl-*sn*-glycero-3-phosphocholine;
POPG, 1-palmitoyl-2-oleoyl-*sn*-glycero-3-phospho-(1'-*rac*-glycerol) (sodium salt);
TMD, Transmembrane Domain;
EPR,electron paramagnetic resonance;
DEER, double electron-electron resonance.
.

References

1. Abbott, G. W. (**2016**) KCNE1 and KCNE3: The yin and yang of voltage-gated K+ channel regulation, *Gene 576*, 1-13.
2. Lewis, A., McCrossan, Z. A., and Abbott, G. W. (**2004**) MinK, MiRP1, and MiRP2 diversify Kv3.1 and Kv3.2 potassium channel gating, *Journal of Biological Chemistry 279*, 7884-7892.
3. Schroeder, B. C., Waldegger, S., Fehr, S., Bleich, M., Warth, R., Greger, R., and Jentsch, T. J. (**2000**) A constitutively open potassium channel formed by KCNQ1 and KCNE3, *Nature 403*, 196-199.
4. Barro-Soria, R., Ramentol, R., Liin, S. I., Perez, M. E., Kass, R. S., and Larsson, H. P. (**2017**) KCNE1 and KCNE3 modulate KCNQ1 channels by affecting different gating transitions, *Proceedings of the National Academy of Sciences of the United States of America 114*, E7367-E7376.
5. Ohno, S., Toyoda, F., Zankov, D. P., Yoshida, H., Makiyama, T., Tsuji, K., Honda, T., Obayashi, K., Ueyama, H., Shimizu, W., Miyamoto, Y., Kamakura, S., Matsuura, H., Kita, T., and Horie, M. (**2009**) Novel KCNE3 Mutation Reduces Repolarizing Potassium Current and Associated With Long QT Syndrome, *Human Mutation 30*, 557-563.
6. Lundquist, A. L., Manderfield, L. J., Vanoye, C. G., Rogers, C. S., Donahue, B. S., Chang, P. A., Drinkwater, D. C., Murray, K. T., George Jr, and L., A. (**2005**) Expression of multiple KCNE genes in human heart may enable variable modulation of I(Ks), *J Mol Cell Cardiol. 38*, 277-287.
7. Grahammer, F., Warth, R., Barhanin, J., Bleich, M., and Hug, M. J. (**2001**) The small conductance K+ channel, KCNQ1 - Expression, function, and subunit composition in murine trachea, *Journal of Biological Chemistry 276*, 42268-42275.
8. Sun, J., and MacKinnon, R. (**2020**) Structural Basis of Human KCNQ1 Modulation and Gating, *Cell 180*, 1-8.
9. Barro-Soria, R., Perez, M. E., and Larsson, H. P. (**2015**) KCNE3 acts by promoting voltage sensor activation in KCNQ1, *Proceedings of the National Academy of Sciences of the United States of America 112*, E7286-E7292.
10. Preston, P., Wartosch, L., Gunzel, D., Fromm, M., Kongsuphol, P., Ousingsawat, J., Kunzelmann, K., Barhanin, J., Warth, R., and Jentsch, T. J. (**2010**) Disruption of the K+ Channel beta-Subunit KCNE3 Reveals an Important Role in Intestinal and Tracheal Cl- Transport, *Journal of Biological Chemistry 285*, 7165-7175.
11. Boucherot, A., Schreiber, R., and Kunzelmann, K. (**2001**) Regulation and properties of KCNQ1 (K(v)LQT1) and impact of the cystic fibrosis transmembrane conductance regulator, *Journal of Membrane Biology 182*, 39-47.
12. Lundby, A., Ravn, L. S., Svendsen, J. H., Haunso, S., Olesen, S. P., and Schmitt, N. (**2008**) KCNE3 mutation V17M identified in a patient with lone atrial fibrillation, *Cellular Physiology and Biochemistry 21*, 47-54.
13. Abbott, G. W., Butler, M. H., and Goldstein, S. A. N. (**2006**) Phosphorylation and protonation of neighboring MiRP2 sites: function and pathophysiology of MiRP2-Kv3.4 potassium channels in periodic paralysis, *Faseb Journal 20*, 293-301.

14. Delpon, E., Cordeiro, J. M., Nunez, L., Thomsen, P. E. B., Guerchicoff, A., Pollevick, G. D., Wu, Y. S., Kanters, J. K., Larsen, C. T., Burashnikov, E., Christiansen, M., and Antzelevitch, C. (**2008**) Functional Effects of KCNE3 Mutation and Its Role in the Development of Brugada Syndrome, *Circulation-Arrhythmia and Electrophysiology 1*, 209-218.
15. Zhang, D. F., Liang, B., Lin, J., Liu, B., Zhou, Q. S., and Yang, Y. Q. (**2005**) KCNE3 R53H substitution in familial atrial fibrillation, *Chinese Medical Journal 118*, 1735-1738.
16. Kroncke, B. M., Van Horn, W. D., Smith, J., Kang, C. B., Welch, R. C., Song, Y. L., Nannemann, D. P., Taylor, K. C., Sisco, N. J., George, A. L., Meiler, J., Vanoye, C. G., and Sanders, C. R. (**2016**) Structural basis for KCNE3 modulation of potassium recycling in epithelia, *Science Advances 2*.
17. Sansom, M. S. P., Bond, P. J., Deol, S. S., Grottesi, A., Haider, S., and Sands, Z. A. (**2005**) Molecular simulations and lipid-protein interactions: potassium channels and other membrane proteins, *Biochemical Society Transactions 33*, 916-920.
18. Ramelot, T. A., Yang, Y., Sahu, I. D., Lee, H.-W., Xiao, R., Lorigan, G. A., Montelione, G. T., and Kennedy, M. A. (**2013**) NMR structure and MD simulations of the AAA protease intermembrane space domain indicates peripheral membrane localization within the hexaoligomer, *Febs Letters 587*, 3522-3528.
19. Sahu, I. D., Craig, A. F., Dunagum, M. M., McCarrick, R. M., and Lorigan, G. A. (**2017**) Characterization of bifunctional spin labels for investigating the structural and dynamic properties of membrane proteins using EPR spectroscopy, *Journal of Physical Chemistry B 121*, 9185-9195.
20. Weng, J., and Wang, W. (2013) Molecular Dynamics Simulation of Membrane Proteins, In *Protein Conformational Dynamics* (Han, K.-l., and Zhang, X., and Yang, M.-j., Eds.), pp 305-329.
21. Muller, M. P., Jiang, T., Sun, C., Lihan, M. Y., Pant, S., Mahinthichaichan, P., Trifan, A., and Tajkhorshid, E. (**2019**) Characterization of Lipid-Protein Interactions and Lipid-Mediated Modulation of Membrane Protein Function through Molecular Simulation, *Chemical Reviews 119*, 6086-6161.
22. Pandey, B., Grover, A., and Sharma, P. (**2018**) Molecular dynamics simulations revealed structural differences among WRKY domain-DNA interaction in barley (Hordeum vulgare), *Bmc Genomics 19*.
23. Li, M. H., Luo, Q. A., Xue, X. G., and Li, Z. S. (**2011**) Molecular dynamics studies of the 3D structure and planar ligand binding of a quadruplex dimer, *Journal of Molecular Modeling 17*, 515-526.
24. Sonntag, Y., Musgaard, M., Olesen, C., Schiott, B., Moller, J. V., Nissen, P., and Thogersen, L. (**2011**) Mutual adaptation of a membrane protein and its lipid bilayer during conformational changes, *Nature Communications 2*.
25. Phillips, J. C., Braun, R., Wang, W., Gumbart, J., Tajkhorshid, E., Villa, E., Chipot, C., Skeel, R. D., Kalé, L., and Schulten, K. (**2005**) Scalable molecular dynamics with NAMD, *J. Comput. Chem. 26*, 1781–1802.
26. MacKerell, A. D., Bashford, D., Bellott, M., Dunbrack, R. L., Evanseck, J. D., Field, M. J., Fischer, S., Gao, J., Guo, H., Ha, S., Joseph-McCarthy, D., Kuchnir, L., Kuczera, K., Lau, F. T. K., Mattos, C., Michnick, S., Ngo, T., Nguyen, D. T., Prodhom, B., Reiher, W. E., Roux, B., Schlenkrich, M., Smith, J. C., Stote, R., Straub, J., Watanabe, M., Wiorkiewicz-Kuczera, J., Yin, D., and Karplus, M. (**1998**) All-atom empirical potential for molecular modeling and dynamics studies of proteins, *Journal of Physical Chemistry B 102*, 3586-3616.
27. MacKerell, A. D., Feig, M., and Brooks, C. L. (**2004**) Improved treatment of the protein backbone in empirical force fields, *Journal of the American Chemical Society 126*, 698-699.
28. Asare, I. K., Perez, A., Garcia, A. B., Cruz, M. F., Moura, A. C. M., Campbell, C. C., Scheyer, M., Alao, J. P., Kravats, A. N., Lorigan, G. A., Sahu , and D., I. (**2022**) Studying structural and dynamic properties of KCNE3 in different membrane mimic systems using molecular dynamics simulations, *Biophysical Journal 121*, 196a.
29. Jo, S., Kim, T., Iyer, V. G., and Im, W. (**2008**) Software news and updates - CHARNIM-GUI: A web-based grraphical user interface for CHARMM, *Journal of Computational Chemistry 29*, 1859-1865.
30. Humphrey, W., Dalke, A., and Schulten, K. (**1996**) VMD-Visual Molecular Dynamics, *J. Molec.Graphics 14*, 33-38.
31. Schwieters, C. D., and Clore, G. M. (**2001**) The VMD-XPLOR visualization package for NMR structure refinement, *Journal of Magnetic Resonance 149*, 239-244.
32. Jo, S., Kim, T., and Im, W. (**2007**) Automated Builder and Database of Protein/Membrane Complexes for Molecular Dynamics Simulations, *Plos One 2*.
33. Essmann, U., Perera, L., Berkowitz, M. L., Darden, T., Lee, H., and Pedersen, L. G. (**1995**) A SMOOTH PARTICLE MESH EWALD METHOD, *Journal of Chemical Physics 103*, 8577-8593.
34. ([34.) Barrett, P. J., Song, Y., Van Horn, W. D., Hustedt, E. J., Schafer, J. M., Hadziselimovic, A., Beel, A. J., and Sanders, C. R. (**2012**) The Amyloid Precursor Protein Has a Flexible Transmembrane Domain and Binds Cholesterol, *Science 336*, 1168-1171.
35. Sahu, I. D., Craig, A. F., Dunagan, M. M., Troxel, K. R., Zhang, R., Meiberg, A. G., Harmon, C. N., MaCarrick, R. M., Kroncke, B. M., Sanders, C. R., and Lorigan, G. A. (**2015**) Probing Structural Dynamics and Topology of the KCNE1 Membrane Protein in Lipid Bilayers via Site-Directed Spin Labeling and Electron Paramagnetic Resonance Spectroscopy, *Biochemistry 54*, 6402-6412.

579 36. Kang, C. B., Vanoye, C. G., Welch, R. C., Van Horn, W. D., and Sanders, C. R. (**2010**) Functional Delivery of a Membrane
580 Protein into Oocyte Membranes Using Bicelles, *Biochemistry 49*, 653-655.